Development and testing of the new SRT receiver and modeling the Sun

Divyanshu Vats
University of Texas at Austin

Alan E. E. Rogers
MIT Haystack Observatory

***Abstract*— The receiver for the Small Radio Telescope (SRT) is being upgraded to a new, digital receiver to enable interferometry experiments. Part of our summer work was to test and debug this new receiver. Initial tests were done by observing the Sun using a short baseline of about 50 feet. During the recent high solar activity, the baseline was increased to about 200 feet. To compensate for the deviation from the typical solar behavior, we studied the effects of limb brightening and sunspots on the cross-correlation values. Additional summer work involved the layout and design of the new ground control unit for the SRT.**

I. INTRODUCTION

The Small Radio Telescope (SRT) is being upgraded to an interferometry based receiver. This will allow students to easily perform interferometry and interactively learn radio astronomy. The system isn't complete and still in the testing stage. Much of the work presented here is to check for the validity of the cross-correlation values obtained from the new receiver on observing the Sun. There were several factors that caused the values to deviate from the theoretical value and those will be discussed in the paper. Some work was also done in designing a new ground control unit for the SRT so that it can drive motors that run in both azimuth and elevation at the same time. For this we are planning to use a PWMPAL which has the capability of doing background counting of pulses coming out of the motors. In addition, an analog to digital converter will be used to measure the current going through motors.

II. PREVIOUS WORK

The SRT has been successfully used in interferometry using a Yagi-Uda Array and another SRT. Both methods are adding interferometers and require a setup of a circuit in order for the signals to correlate themselves. In order for the experiment to work, the power level of the signal coming from the antennas should be the same. In addition the power on-source and power off-source should also be the same. Once everything is set up properly, you see fringes which signify that the interferometer is working properly.

Before experimenting with the new receiver, the adding interferometer was set up. This was done to get a general feeling of interferometry before the much more complicated way was used. The fringes obtained are shown in figure 1, but this was only during the day time. As the day progressed the fringes disappeared because the baseline, distance between the antennas, visible to the Sun increased. It is also believed that the Sun was very quite during the time of the experiment.

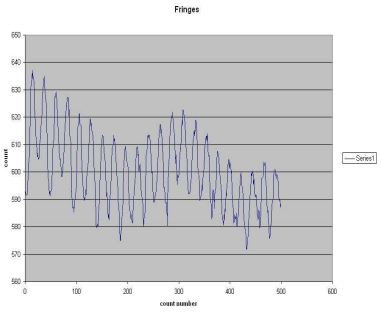

Fig. 1. fringes seen with the adding interferometer

III. THE NEW RECEIVER

The following sections will talk in detail about the new receiver for the SRT.

A. Design

The block diagram and picture of the receiver are shown in figure 2 and 3 respectively. All the hardware needed has been put into one box. The system has a motherboard which communicates to the hardware using USB 2.0 and runs under Linux Gentoo. The system is capable of performing interferometry and thus has an inbuilt correlator that operates in real time. For the correlation to be fast enough, a Digital Signal Processor (DSP)

has been used to crunch the fast fourier transforms necessary for the calculation of cross-correlation. All the embedded code in the DSP is written in assembly and C. Furthermore, the receiver has a GPS timing capability which is yet to be tested and still in the development stage.

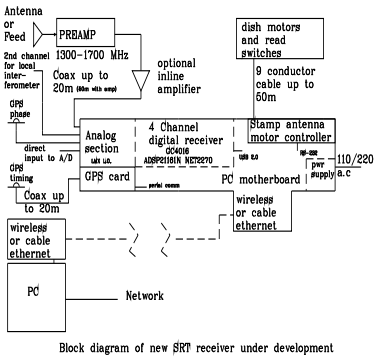

Fig. 2. Block diagram of the receiver

The motherboard has a network card which opens port 22 for ssh to the outside world. This will enable students to access the system remotely and not go through the process of setting up the SRT at there school or college. Students might want to see whether the SRT is actually moving when they command it to do so and this can be done by setting up a webcamera to point at the antenna.

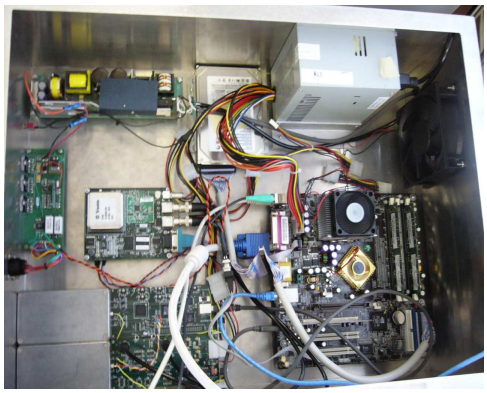

Fig. 3. Picture of the receiver

B. Interface

The previous interface was written in Java. Although Java is portable to multiple operating systems, its execution speed is slow as compared to other languages. Java is ideal for windows, but when it comes to linux it is better to use GTK. A screenshot of the new interface is shown in figure 4. It is pretty much the same as the previous one except that it has an interferometry mode. This lets you see the correlation values, phase values, and also the spectrum from both the signals.

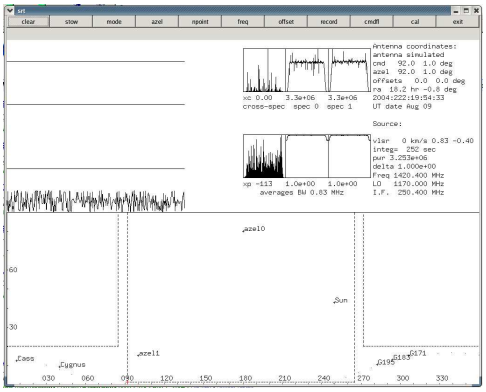

Fig. 4. The new interface

IV. SETUP

Our setup is shown in figure 5. We are using one fixed SRT and another mobile SRT.

Fig. 5. Picture of the setup

We changed the position of the mobile SRT for variable baselines. The receiver box was kept in the trailer and the signals from the SRTs came into the receiver through coaxial cables. Since the mobile SRT is very far from the trailer, the signal coming from it was delayed and we compensated for this in software. Due to possible degradation in the signal, we also put in three Local Noise Amplifiers (LNAs) to increase the strength of the signal.

V. RESULTS

The new receiver was tested by analyzing the data obtained on tracking the Sun. The graphs of the cross-correlation and phase values are presented in this section. In order to compensate for the deviations in the ideal behavior, we created a model for fitting the theoretical data to match the measured data. In addition, we present some simple algorithms that can enable us to calculate important parameters such as the azimuth between antennas, the distance between antennas, and the sunspot area.

A. Theory

Cross-correlation is the standard method to determine the extent to which two signals are correlated.

Let $x(t)$ and $y(t)$ be the signals coming from the two antennas. Then $X(\omega)$ and $Y(\omega)$ are the respective fourier transforms. These calculations are done in the DSP using an efficient algorithm.

We calculate the cross spectrum:

$$S(\omega) = X(\omega)Y^*(\omega)$$

Summing over frequency with delay constant we get:

$$c = \sum_{\omega} S(\omega)e^{i\omega\tau}$$

$$p_x = \sum_{\omega} X(\omega)X^*(\omega) \qquad p_y = \sum_{\omega} Y(\omega)Y^*(\omega)$$

Normalizing the data we get the final correlation and phase as

$$\rho = \frac{c}{\sqrt{p_x p_y}} \qquad phase = tan^{-1}\left(Im\{c\}, Re\{c\}\right)$$

The cross-correlation of the two signals from the antennas is same as the visibility function of the Sun. This function depends on the vector distance between the antennas, which is often referred to as the baseline. If the Sun is assumed to be a uniform disc, then the visibility function, V, is given by $V = \frac{2\,J_1(b\,R)}{b\,R}$, where $J_1(\cdot) = 1$st order bessel function, $b =$ baseline in wavelengths, and $R =$ angular radius of the Sun. This function is plotted in figure 6, which also shows the difficulty of getting a high correlation value for large baselines.

For a particular baseline, the visibility function will vary with time because the earth is rotating. This causes the effective baseline, the distance between antennas as seen from the Sun, to change. The measured baseline, actual distance between the antennas, becomes equal to the effective baseline when the Sun is in such a position that the signals coming from it are not delayed. At this point the correlation value from the graph should correspond to the measured value. All this works well assuming that the Sun is a uniform disc, but in reality there are some deviations from the ideal behavior.

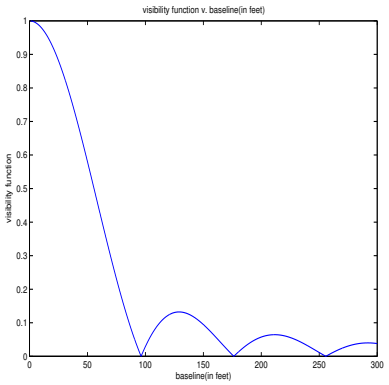

Fig. 6. Graph of the visibility function

B. Measured Values

We started taking data with a 53 feet baseline. This gave us reasonably high correlation values which was sufficient to test for the systems accuracy. There were several difficulties with the mobile SRT, but we were still able to get enough data for comparsions. Figure 7 shows four curves for the 53 feet baseline: day 183, 189, 190, and 191. The experiment on day 190 was started at a later time which is why we see a dip in the beginning. The curves shown were obtained by fitting the data to a third degree polynomial.

A good test of whether the system is accurate or not, is to check for consistency in the curve. Clearly the curves follow almost the same shape and the slight differences can be accounted for change in activity of the Sun. The graphs for day 203 and day 204 were taken at a 200 feet baseline. From figure 1, you would expect the values to be less than 0.1, but they are almost four times of that. This is because the Sun was highly active during these days. Here also you see consistency in the curves, which suggests the system is fairly accurate. Remarkably the correlation values during this high solar activity was about 0.7 with a 53 feet baseline.

The values shown in figure 7 are actually the magnitude of correlation values. In reality, cross-correlation is a complex number and thus has an associated phase. The phase values for day 183 and day 189 are shown in figure 8a and 8b respectively. As we will see later sections,

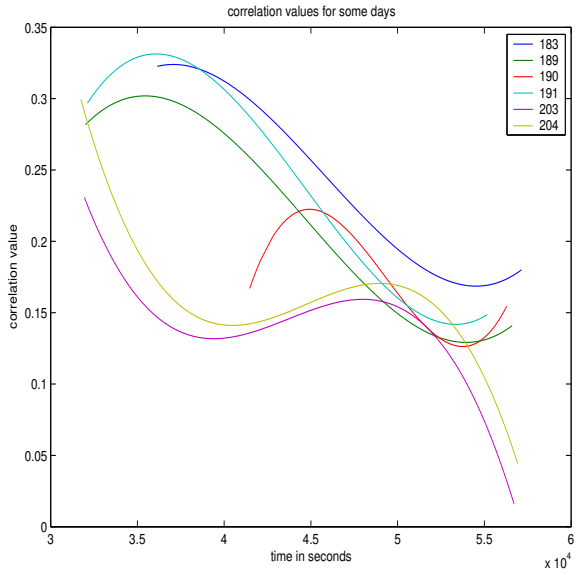

Fig. 7. Measured correlation values on different days

these values closely match the theoretical value of the phase. On increasing the baseline to 200 feet, the period of the phase became very small and was only visible on zooming in the graph.

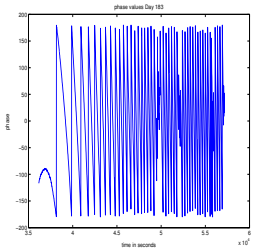

(a) Measured phase for day 183

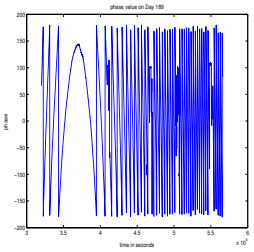

(b) Measured phase for day 189

Fig. 8. Phase values on Day 183 (a) and Day 189 (b)

C. Analysis

The first step in analyzing the data is to calculate the theoretical value of the correlation and phase. This was done by writing a program in C that could generate the theoretical correlation and phase for any day. Figure 9 shows the theoretical and measured correlation values along with the theoretical and measured phase.

As can be seen from the figure, the phase values match very well, but the correlation values have a huge difference. It is believed that this difference is because of the limb brightening in Sun and the noise in the receiver. Limb brightening is when the energy of the

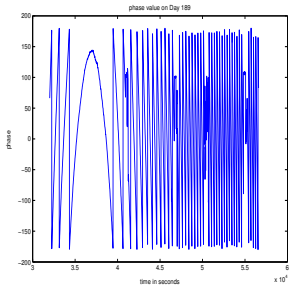

(a) Meausred phase for day 189

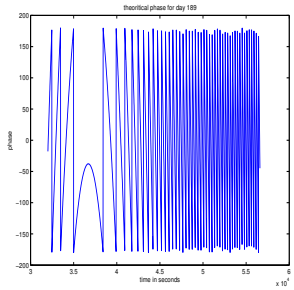

(b) Theoritical phase for day 189

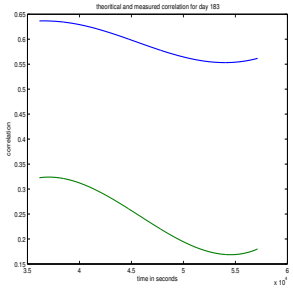

(c) correlation values for day 183

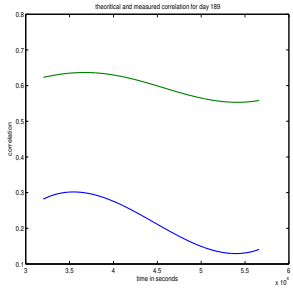

(d) correlation values for day 189

Fig. 9. Comparsion of measured and theoretical values

Sun at the edges increases and thus deviates from the uniform disc model. We tried to compensate these effects in the program, but it is difficult to do so because of the large receiver noise. Since the Sun was very quite during that time, the noise in the receiver has a much more pronounced effect. Thus it is better to model the Sun during its high activity when the receiver noise gets overshadowed by the high signal energy.

This happened during the week of 18th July when a sunspot on the Sun was so large, that it was visible from the naked eye. Sunspots are areas on the Sun's surface that have a lower temperature than the rest of the surroundings. But in terms radio brightness, these area are very bright and emit a lot of energy.

The correlation values for day 203 are shown in figure 10. As you can see the measured value has a totally different shape than the actual value. The next section describes the modeling techniques that were used to compensate for limb brightening, sunspot effects, and the receiver noise.

D. Modeling the data

After careful observation of the data for the 53 feet baseline, we concluded that the curve drops more rapidly than expected towards the end of the day. A possible reason for this is the long baseline in the Sun's frame of reference. Thus to model the data, it is better to ignore

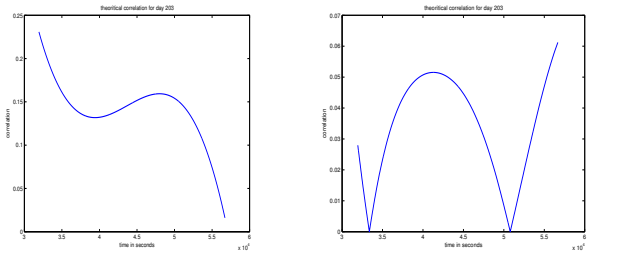

(a) measured correlation for day 203 (b) theoretical correlation for day 203

Fig. 10. Measured and theoretical correlation for day 203

the points during that time and focus on somewhere in the middle.

We decided to model the data for day 203 using 1250 points which corresponds to 12500 seconds as the system records data every 10 seconds. The parameters involved in modeling the Sun are; thickness of limb brightening, relative energy due to the limb brightening, sunspot area, and relative energy due to the sunspot. The area of the sunspot for day 203, 22nd July, 2004 was found to be 2847.62 microhemisphere.

We assumed the sunspot was near the center of the Sun and formed another uniform disc over there. Let r_x be the theoretical angular sunspot radius, r_s be the angular Sun radius, A_x be the area of the sunspot, and A_s be the area of the Sun assumed to be a uniform disc. Then,

$$\begin{aligned}
\frac{r_x}{r_s} &= \sqrt{\frac{A_x}{A_s}} \\
r_x &= \sqrt{\frac{2847.62 \cdot 2 \cdot \pi \cdot R^2 \cdot 10^{-6}}{\pi \cdot R^2}} \cdot r_s \\
r_x &= \sqrt{2847.62 \cdot 2 \cdot 10^{-6}} \cdot r_s \\
r_x &\simeq 0.019
\end{aligned}$$

Thus, theoretically, the sunspot has a radius of 0.019°. Initially we modeled the data by assuming some arbitrary values for the other parameters. When we knew how each value affected the curve, we wrote a program to find the minimum model based on the least square distance. The modeled data is shown in figure 11, along with the measured data.

They are very close suggesting that the parameters might be right. The only problem with this modeling is that we only have one condition to satify and there are three variables. So there are many solutions possible, but we tried to narrow ourself to the more realistic solution.

The values obtained can be visually seen in figure 12.

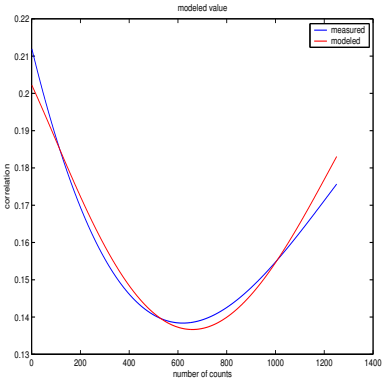

Fig. 11. Modeled value

It shows a theoretical figure of the Sun with the sunspot and the limb brightened area. It also tries to tell us the change in brightness at different locations. We found that the brightness on the sunspot was thirty five times that of the rest of the surface and the limb brightening was five times that of the rest of the area. The thickness of limb brightening was about 22 percent of the angular radius of the Sun.

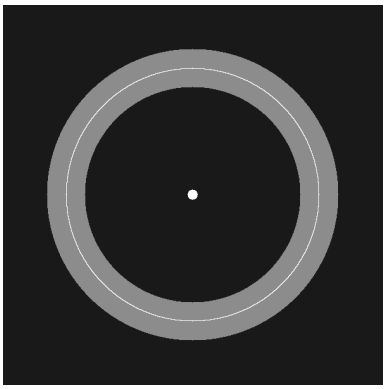

Fig. 12. Model of the Sun

When we took measuremeants with the 53 feet baseline, the sunspot area was almost zero. So in this case we assume that only limb brightenining was there. On applying the model to the 183rd day we get the curve shown in figure 13.

Unlike the previous case, the modeled value is shifted upwards by some amount. This shift can be accounted as the receiver noise because during this time the Sun's activity was very low and thus the noise was much more pronounced. After shifting, the best fit occurs when the modeled value is moved down about 0.08. Thus we can say that the receiver accounts for a degradation in the

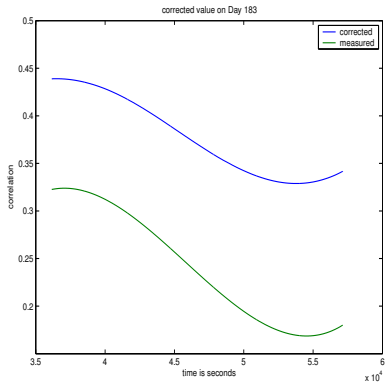

Fig. 13. Modeling data on 183rd day

values by an amount of 0.08.

So now we have a complete model of the Sun plus the noise in the receiver. With this information we can model other sets of data that we collected.

We don't claim that the model of the Sun calculated is correct. In fact it is far from correct because the sunspot is not actually near the center. With more baselines we may have been able to find the actual sunspot location and this can be part of a future project. But the model can be used to approximately correct for the measured values and this can very useful in analysis.

E. Measuring other values

1) Azimuth: The azimuth between the two antennas can be calculated by looking for the point on the measured data where we acheive a local minima. For this we don't need to model the theoretical value. This was done using MATLAB and C implentation can be written, but it will take more time. The C implementation will require us to use optimum search techniques because we are looking at a lot of data.

2) Baseline: The baseline can also be measure provided we know the azimuth and the receiver noise. As baseline increases, keeping other things the same, the graph moves downward and this amount can only be measured if we know the amount shifted is only due to baseline and not due to any noise.

3) Sunspot Area: A rough idea of Sunspot area can be coined, provided that the sunspot, is large enough. Since the sunspot has the effect of canceling the noise, this situation is very complex and requires more conditions to calculate things effectively.

VI. GROUND CONTROL UNIT

This section talks about the new ground control unit that is being designed for the SRT. The motors are in the process of being replaced so that they can move in both azimuth and elevation at the same time. This requires added functionality in the unit. The planned design of the unit is shown in figure 14. The following sections will discuss the different part that will be used in the new unit.

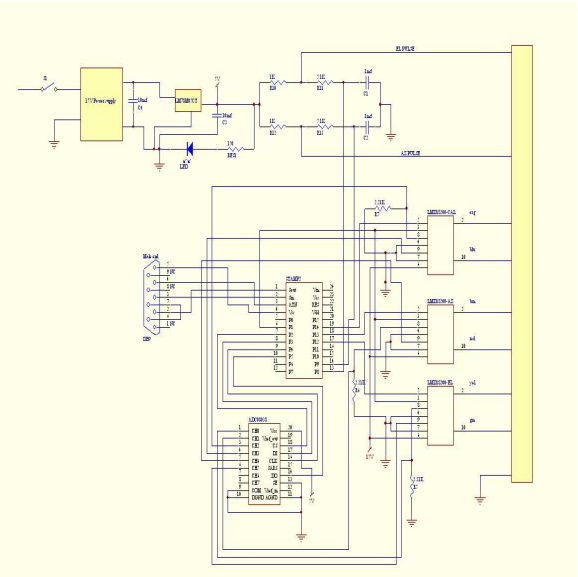

Fig. 14. Block diagram of the ground control unit

A. BASIC STAMP 2

BASIC STAMP 2 is a simple microcontroller that will talk to the rest of the compenents and generate necessary commands for processing. Previously a BASIC STAMP was being used but it had only 8 input/output (IO) pins as opposed to the 16 on the new stamp.

B. PWMPAL

The PWMPAL is an intelligent peripheral that hooks up to the BASIC STAMP 2 and can generate pulse width modulated signals (PWM). It communicates to the stamp using pin 0. Another neat feature of the PWMPAL is that it can do background conting which can be used to count the pulses coming out of the motors. The module was tested for its ability to generate PWM signals. It was also tested for its background couting feature by sending out the PWM signal to the input pin for PWMPAL.

C. LMD18200

This is the main component that drives the motors using the PWM signal that it gets from the PWMPAL. It can also control the direction in which the motors run and also has a current sensing option for measuring the current passing through the motors. The compenent was tested by hooking it up to a motor to make sure that it was generating current according to the duty cycle that was specified. The duty cycle is the amount of time the PWM signal is high.

D. ADC08038

ADC08038 is an eight bit analog to digital converter. It will be used in the unit to measure the amount of current flowing through the motors. This will allow for checking when the motors are not working properly. The current will be measured by using the current sensing pin from the LMD18200. The ADC08038 was tested by seeing whether it could measure certain voltage values. It was also tested for measuring the current values driving the motor. In order for this to work, a 2.21 kΩ resistor was used because the A/D converter can read voltage values in the range of 0 to 5 V.

E. Future work

The main part left is to implement the whole unit through the BASIC STAMP 2. This should be relatively easy as all the parts have been tested and connecting them togather should not be a very difficult job. There are also plans to implement a LabView GUI in order to test the motors comprehensively.

VII. CONCLUSION

The receiver was tested for its correlation values and they seem to be consistent with the theoretical values. By modeling the theoretical values we were able to account for deviations in the ideal behavior of the Sun. This can be an excellent exercise for students and it will also help them understand the basics of interferometry. They will also see the kind of observations one can make by using two SRTs as opposed to using a single SRT for observing the Sun.

The only problem with this is the low correlation values that we got during the experiments. The only time we got good correlation values was when the baseline was short and when there was high solar activity.

VIII. APPENDIX

This section shows some results on applying the complete model to the 53 feet baseline values. All the graphs are shown in figure 15. As you can see the modeled curves are not very accurate but they are close enough. Further accuracy can be acheived if we model the Sun using decimal values. We accounted for only three affects and there might be more deviations in the Sun that we are not aware of. Testing on other data sets will be done to see how accurate the model actually is.

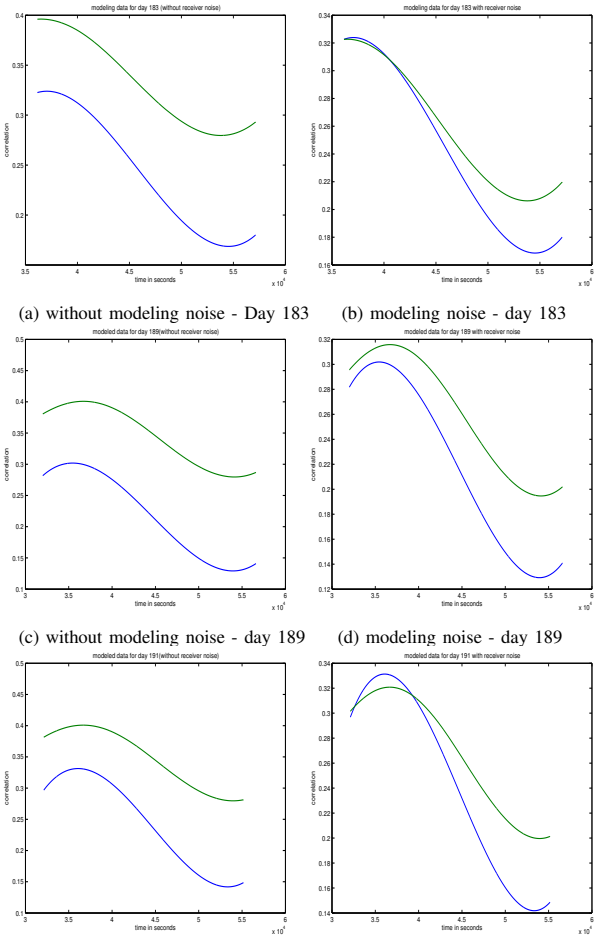

(a) without modeling noise - Day 183 (b) modeling noise - day 183

(c) without modeling noise - day 189 (d) modeling noise - day 189

(e) without modeling noise - day 191 (f) modeling noise - day 191

Fig. 15. Applying the model to different days for 53 feet baseline